Dalton Transactions

Accepted Manuscript

ROYAL SOCIETY OF CHEMISTRY

www.rsc.org/dalton

Synthesis and characterization of three amino-functionalized metal-organic frameworks based on 2-Aminoterephthalic ligand

Ying Yang,[a] Rijia Lin,[a] Lei Ge,[a*] Lei Hou,[b] Paul Bernhardt,[c] Thomas E. Rufford,[a] Shaobin Wang,[d] Victor Rudolph,[a] Yaoyu Wang,[b] Zhonghua Zhu[a*]

[a] *School of Chemical Engineering, The University of Queensland, Brisbane 4072 Australia*

[b] *College of Chemistry & Materials Science, Northwest University, Xi'an 710069, China*

[c] *School of Chemistry and Molecular Biosciences, The University of Queensland, Brisbane 4072 Australia*

[d] *Department of Chemical Engineering, Curtin University, GPO Box U1987, Perth, WA 6845, Australia*

Abstract: The incorporation of Lewis base sites and open metal cation sites into metal-organic frameworks (MOFs) is a potential route to improve selective CO_2 adsorption from gas mixture. In this study, three novel amino-functionalized metal-organic frameworks (MOFs): Mg-ABDC [$Mg_3(ABDC)_3(DMF)_4$], Co-ABDC [$Co_3(ABDC)_3(DMF)_4$] and Sr-ABDC [Sr(ABDC)(DMF)] (ABDC = 2-aminoterephthalate) were synthesized by solvothermal reactions of 2-aminoterephthalic acid (H_2ABDC) with magnesium, cobalt and strontium metal centers, respectively. Single-crystal structure analysis showed that Mg-ABDC and Co-ABDC were isostructural compounds comprising two-dimensional layered structures. The Sr-ABDC contained a three-dimensional motif isostructural with its known Ca analogue. The amino-functionalized MOFs were characterized by powder X-ray diffraction, thermal gravimetric analysis and N_2 sorption. The CO_2 and N_2 equilibrium adsorption capacities were measured at different temperatures (0, 25 and 35 °C). The CO_2/N_2 selectivities of the MOFs were 396 on Mg-ABDC, 326 on Co-ABDC and 18 on Sr-ABDC. Both Mg-ABDC and Co-ABDC exhibit high heats of CO_2 adsorption (> 30 kJ/mol). The Sr-ABDC displays good thermal stability but had a low adsorption capacity resulting from narrow pore apertures.

1. Introduction

MOFs have been identified as potential materials to use in adsorption based CO_2 capture technologies to reduce greenhouse gas emissions from fossil fuel combustion processes.[1-5] Numerous scientific studies have explored techniques to optimize MOFs structures to increase selectivity for CO_2 adsorption from gas mixtures including the control of pore size and shape, ligand functionalization, incorporation of open metal cation sites, and functionalization of the MOF with polar and basic functional groups.[6] We report here the preparation, CO_2 adsorption capacities and selectivity of CO_2 over N_2 of three MOFs with amino-functional groups and open metal sites (Mg^{2+}, Co^{2+} and Sr^{2+}).

The incorporation of polar functional groups, including basic nitrogen-containing groups such as aromatic amines, heterocycles and alkylamines into MOFs has been investigated widely as a strategy to increase the selectivity for CO_2 over other gases.[7-15] The polar nitrogen-containing groups can act as Lewis base sites (LBSs) to enhance CO_2 adsorption due to acid-base interactions between CO_2 (acid) and the basic active centers in addition to the formation of organic carbamates.[5, 16, 17] The LBSs in MOFs may also induce dispersion and electrostatic forces to enhance the CO_2 adsorption selectivity.[17, 18] To incorporate LBSs into the frameworks, MOFs can be functionalized with amino ligands and their derivatives during or after synthesis.[17] 2-aminoterephthalic acid (H_2ABDC) as a derivative of terephthalic acid, has been used extensively as an effective organic building block for construction of extended open frameworks,[6, 8, 19-22] such as IRMOF-3,[23] NH_2-MIL-53,[24] NH_2-UiO(Zr)-66,[11, 25] [Zn-(BDC-NH_2)(TED)$_{0.5}$][26] etc. In these complexes only the carboxylate groups of the deprotonated $ABDC^{2-}$ ligand take part in metal bonding, while the substituted amino groups do not coordinate the metal centers, so these amino groups may act as binding sites and provide strong affinity for CO_2 molecules.[19, 22] Adding amine functionalities to the linkers of IRMOF-1 to produce IRMOF-3 provides 0.4 wt.% improvement in CO_2 uptake at 25 °C and

1.1 bar, even though a decrease in the BET surface area of IRMOF-3 from 2833 to 2160 m^2/g occurred.[23, 27] Compared to MIL-53, amino-MIL-53 using H_2ABDC as the linker shows significant improvement in the selectivity of CO_2/CH_4, from ~7 to almost infinite selectivity at 1 bar. The main reason is that the presence of the amino groups together with the hydroxyl groups remarkably enhances the affinity for CO_2 molecules.[6] Another example is that UiO-66(Zr)-NH_2 shows significant enhancement in adsorption enthalpies and working capacities for CO_2 as well as higher CO_2/CH_4 selectivity though it has the similar physicochemical properties (surface areas and pore volumes) to UiO-66(Zr).[11, 25]

To build open metal sites (OMSs, or unsaturated metal centers, UMCs) in the frameworks is another common approach to improve the affinity and selectivity of MOFs towards CO_2.[28-32] These OMSs are typically obtained upon the desolvation of MOFs, where the solvent molecules (e.g. H_2O, DMF) in the coordination of the metal centers are removed at elevated temperatures and/or under vacuum.[5, 17] The OMSs serve as charge-dense binding sites and interact more strongly with CO_2 in selective gas adsorption, playing an important role in CO_2 separation. Hence, the efficiency of solvent removal significantly affects the application of MOFs in gas adsorption and separation.[33, 34] M_2(dobdc) (M= Mg, Zn, Co, Ni, Fe etc., dobdc= dioxidoterephthalate) structure type represents one of the most well-studied families of MOFs with exposed metal cation sites.[35-42] In this M_2(dobdc) series, frameworks with different metal centers have quite different CO_2 capacities. In addition, the zero-coverage isosteric heat of CO_2 adsorption on this series of materials is significantly affected by the density of metal cation sites, wherein Mg_2(dobdc) showed the highest affinity (-42 kJ/mol), while Zn_2(dobdc) displayed the weakest interactions (-26 kJ/mol) among the compounds studied.[35] The difference in the isosteric heat of adsorption is attributed to the different ionic characters of the metal-oxide bonds. The Mg-O bonds in Mg_2(dobdc) have higher ionic character than Zn-O bonds in Zn_2(dobdc), leading to a higher positive charge density on the

Mg^{2+} metal centers and facilitating a greater degree of polarization on the adsorbed CO_2 molecules.[35, 42] The high density of metal binding sites (4.6 per nm^3) within the one dimensional pore channels of Mg_2(dobdc) provides high adsorption capacity for CO_2, reaching 19.8 wt.% at 23 °C and 1 bar.[35] The outstanding CO_2 adsorption performance makes Mg_2(dobdc) be an excellent adsorbent for CO_2 capture, illustrating the importance of OMSs with high affinity to the selective gas adsorption.

Combining the advantages of the above strategies, CO_2 binding affinity and selectivity of CO_2 over other gases would be significantly enhanced by both polar functional groups and exposed metal cation sites in MOFs. This study aims to prepare novel MOFs with both LBSs and OMSs. Three amino-functionalized MOFs based on Mg, Co and Sr metal centers were first synthesized by the solvothermal method. Their crystal phase, pore structure and thermal stability were intensively investigated. In addition, the potential CO_2 separation by adsorption was also evaluated.

2. Experimental

2.1. Synthesis of MOFs from 2-aminoterephtahlic acid (H_2ABDC)

Reagent grade magnesium nitrate hexahydrate ($Mg(NO_3)_2 \cdot 6H_2O$); cobalt nitrate hexahydrate ($Co(NO_3)_2 \cdot 6H_2O$); strontium nitrate ($Sr(NO_3)_2$); 2-aminoterephthalic acid (H_2ABDC); N,N-dimethylformamide (DMF); ethanol and methanol from Sigma-Aldrich were used without further purification.

The MOFs were prepared through solvothermal reactions of the H_2ABDC and each of the metal nitrate salts in ethanol/DMF solution according to the ratios shown in Table 1. In each synthesis the reagents were stirred for 10 min at room temperature then transferred to a 15 ml Teflon-lined autoclave and heated at the desired reaction temperature (90 °C for Mg-ABDC; 125 °C for both Co-ABDC and Sr-ABDC) under autogenous pressure for 48 hr. The heating

rate was 0.5 °C/min or 1 °C/min. The solids precipitated in the solvothermal reactions were collected by filtration, washed in DMF and rinsed three times in methanol over two days. The obtained crystals were dried at 60 °C in a vacuum oven.

Table 1 Solvothermal synthesis conditions for amino-functionalized MOFs.

Frameworks	$Mg_3(ABDC)_3(DMF)_4$	$Co_3(ABDC)_3(DMF)_4$	Sr(ABDC)(DMF)
Sample ID	Mg-ABDC	Co-ABDC	Sr-ABDC
H_2ABDC	0.0724 g (0.4 mmol)	0.0362 g (0.2 mmol)	0.0362 g (0.2 mmol)
DMF (ml)	6.0	7.0	6.0
Ethanol (ml)	3.0	2.0	3.0
Metal nitrate	0.204 g (0.8 mmol) $(Mg(NO_3)_2{\cdot}6H_2O)$	0.116 g (0.4 mmol) $(Co(NO_3)_2{\cdot}6H_2O)$	0.0846 g (0.4 mmol) $(Sr(NO_3)_2)$
Reaction temperature (°C)	90	125	125
Heating rate (°C/min)	1	0.5	1
Crystals color	Burly wood	Dark violet	Light brown

2.2. Characterization

Single-crystal structure analyses were performed on an Oxford Diffraction Gemini CCD Diffractometer (employing either Mo-Kα or Cu-Kα radiation) operating in the ω scan mode. The structures were solved by direct methods with SHELXS and refined with SHELXL.[43] Crystallographic data are provided in Table 2.

Table 2 Crystallographic Data for M-ABDC (M=Mg, Co, Sr).

Frameworks	$Mg_3(ABDC)_3(DMF)_4$	$Co_3(ABDC)_3(DMF)_4$	Sr(ABDC)(DMF)
Formula	$C_{36}H_{43}Mg_3N_7O_{16}$	$C_{36}H_{43}Co_3N_7O_{16}$	$C_{11}H_{12}N_2O_5Sr$
FW, g/mol	902.74	1006.56	339.86
Space Group	*Pbca* (No. 61)	*Pbca* (No. 61)	*Pmnb* (No. 62)

T, K	190	190	190
a, Å	18.061(2)	18.128(2)	18.267(1)
b, Å	26.186(7)	25.454(2)	7.3169(3)
c, Å	9.753(3)	9.778(1)	9.9574(6)
Volume, Å^3	4604(2)	4512.2(8)	1330.9(1)
Z	4	4	4
ρ_{calc}, g/cm^3	1.302	1.482	1.696
μ, mm^{-1}	1.231	9.179	4.068
λ, Å	1.54184	1.54184	0.71073
Reflections measured	13577	6778	3717
Independent Reflections	3650	2814	1587
R(int)	0.0996	0.0557	0.0392
Goodness-of-fit on F^2	1.057	1.096	1.228
$R_1{}^a$, $wR_2{}^b$ [I>2σ(*I*)]	0.1497, 0.3414	0.0959, 0.2455	0.0703, 0.1470
CCDC no.	1016534	1016535	1016536

$^aR_1 = \sum(||F_0| - |F_c||) / |F_0|$; $^bwR_2 = [\sum w(F_0^2 - F_c^2)^2 / \sum w (F_0^2)^2]^{1/2}$

Powder X-ray diffraction (PXRD) patterns were collected on a Bruker Advanced X-ray Diffractometer (40 kV, 30 mA) with Cu Kα radiation (λ = 1.5406 Å) operating in the 2θ range from 5 to 50 ° with a scan speed of 0.3 s/step and a step size of 0.2 °. The recorded patterns were compared with the simulated patterns from single crystal data using the Mercury program.[44] Optical images of Mg-ABDC, Co-ADBC and Sr-ABDC crystals were collected on an optical microscope at 200 times magnification using a bright-field operating mode, and then the photos were taken through the ocular lens manually by a digital camera.

Thermal stability of the amino-functionalized MOFs was measured in air with a heating rate of 5 °C/min from 50 to 700 °C on a Perkin Elmer STA 6000 Thermo Gravimetric Analyzer (TGA). A Micromeritics TriStar II 3020 surface area and porosity analyzer was used to measure (i) N_2 sorption isotherms at -196 °C and relative pressures of P/P_0=0.005 to 0.995 for the determination of pore structures and (ii) N_2 and CO_2 adsorption isotherms at 0 and 25 °C

at absolute pressures from 3.5 to 132.0 kPa to evaluate the adsorbents' selectivity for CO_2. Prior to the N_2 sorption measurements, about 0.1 g of each sample was degassed under vacuum for 24 h at the following temperatures: Mg-ABDC at 120 °C, Co-ABDC at 150 °C and Sr-ABDC at 300 °C. The sample tube was back filled with helium before removing from the degasser. Specific surface areas were calculated from the N_2 adsorption isotherm using the Brunauer, Emmett and Teller (BET) equation and the total pore volume was determined at P/P_0=0.995. After N_2 adsorption, the sample was regenerated at 100 °C under a pressure of 1.5 Pa (until the pressure was stable) and then used for the CO_2 adsorption measurements. The measurement temperatures of 0 and 25 °C in the TriStar II 3020 were achieved by immersion of sample tubes in a Dewar connected to a circulating water bath (variation in temperatures ±0.1 °C). CO_2 desorption isotherms were collected by decreasing the system pressure to 3.5 kPa in a series of small pressure steps.

3. Results and discussion

3.1. Structural Description of M-ABDC (M = Mg, Co, Sr)

Single crystal X-ray diffraction indicated that Mg-ABDC and Co-ABDC coordination polymers are isostructural and based on a centrosymmetric, trimetallic cluster with the central metal occupying a centre of symmetry in a near ideal octahedral MO_6 environment and a pair of symmetry related distal metal ions on general sites. As can be seen in Fig.1, all O-donors to the central metal ion are from carboxylate functional groups; four of them binding in a μ_2-O:O' mode and two in a μ_2-O mode. The symmetry related distal metal ions bear four carboxylate O-donors (bridged to the central metal ion) and two monodentate O-bound DMF ligands and their coordination geometries are distorted octahedral. The trinuclear $[M_3(CO_2)_6]$ secondary building unit (SBU) is connected by six ABDC linkers to produce a two-dimensional 3^6 layer parallel to the *ac* plane. There is considerable disorder in both structures

affecting the precision of the final result. Both DMF ligands adopt different positions in the Co structure with similar occupancies (40-60%) while in the Mg structure one coordinated DMF appears to be ordered (but with high thermal parameters) while the other is disordered over two positions. Coupled with this the aromatic amino groups are disordered. The ABDC ligand situated on a centre of symmetry necessarily has the amino group disordered between two symmetry related positions while the ABDC ligand on a general site finds the amino group disordered over three of the four available positions *ortho* to a carboxylate group each at 1/3 occupancy.

In Sr-ABDC, X-ray diffraction reveals a quite different structure: both Sr atom and ABDC ligand occupy a centre of symmetry while a coordinated DMF is disordered about a crystallographic mirror plane. The complex is isostructural with calcium-based MOFs [Ca(ABDC)(DMF)] reported by Liang et al.[45] The Sr(II) ions are eight-coordinated comprising two η^2 (chelating) carboxylates which also bridge a neighboring Sr ion (μ_2-η^1:η^2), two monodentate bridging O-atoms from the same symmetry related carboxylates and two O-atoms from O-bound DMF (which also bridge adjacent Sr ions), generating a distorted bicapped trigonal antiprismatic geometry. A 1D metal-carboxylate chain along the *a* axis is formed, in which one oxygen atom of a DMF ligand bridges two Sr(II) atoms. The chains are further extended by H_2ABDC linkers to generate a 3D framework.

For the structures of Mg-ABDC and Co-ABDC, there are no solvent accessible voids in the structure and no channels along the *b* axis, owing to the dislocation of the neighboring layers along this direction. Notably, the DMF ligands of the distal metal atoms induce large separations of the adjacent layer along the *b* axis. Artificial removal of the DMF ligands from the model leaves 52.7% void volume for the Mg structure and 47.3% for the Co structure as calculated by PLATON[46] between the two layers. The distance between the two layers is

about 4.7 Å after subtracting the van der Waals radii of the atoms. For the case of Sr-ABDC, a rhomboidal channel about 4.6×3.6 $Å^2$ (excluding van der Waals radius) is produced along the *a* axis, in which the DMF ligands are accommodated. Upon (artificially) removing the DMF ligands from the model, the channel has a free void of 35.0%[46] with -NH_2 groups of H_2ABDC located along the wall. The coordinated DMF molecules point toward the channels. The amino groups of the ABDC ligands which extend into the channels are responsible for the small channels and lack of void space.[45] As found in the Mg and Co structures DMF ligand is disordered, in this case a mirror plane and the aromatic amino group are disordered between two centrosymmetrically related positions.

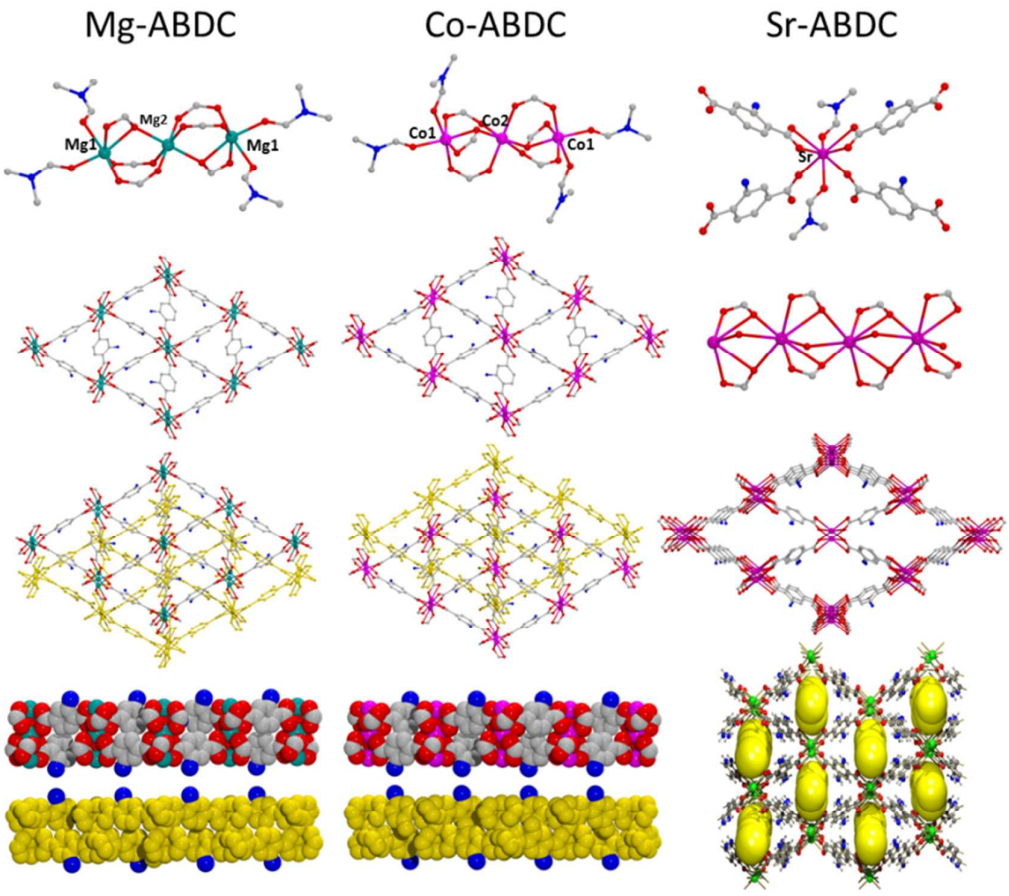

Fig. 1 Structural descriptions of M-ABDC (M=Mg, Co, Sr) (H atoms are omitted and N atoms are marked in blue).

To conclude, the different channel size and void space in the three amino-functionalized frameworks would affect their adsorption performance. In addition, as DMF solvent molecules complete the coordination sphere of the metal (II) ions in these MOFs, the OMSs would be expected to generate in the frameworks upon the effective removal of the DMF molecules by solvent-exchange and evacuation.

3.2. Morphology of M-ABDC (M = Mg, Co, Sr)

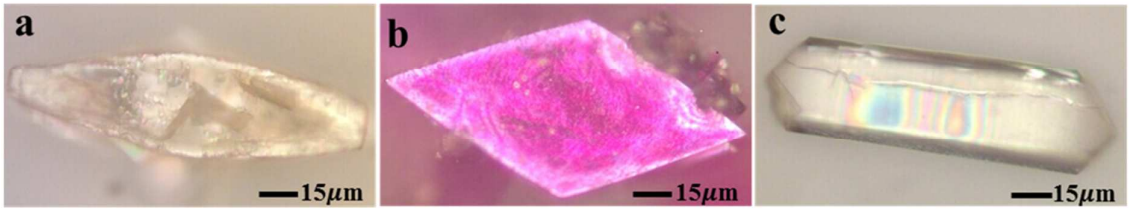

Fig. 2 Optical images at 200x magnification of (a) Mg-ABDC, (b) Co-ABDC and (c) Sr-ABDC.

Optical images of Mg-ABDC, Co-ADBC and Sr-ABDC crystals are shown in Fig. 2. The crystal shapes are consistent with the analytic structures determined by SXRD. The crystals of Mg-ABDC and Co-ABDC have similar rhombus shape and size. The Sr-ABDC crystals are light brown, rods. The colors of the three MOFs are related to the metal cations in each framework.

3.3. PXRD patterns of M-ABDC (M = Mg, Co, Sr)

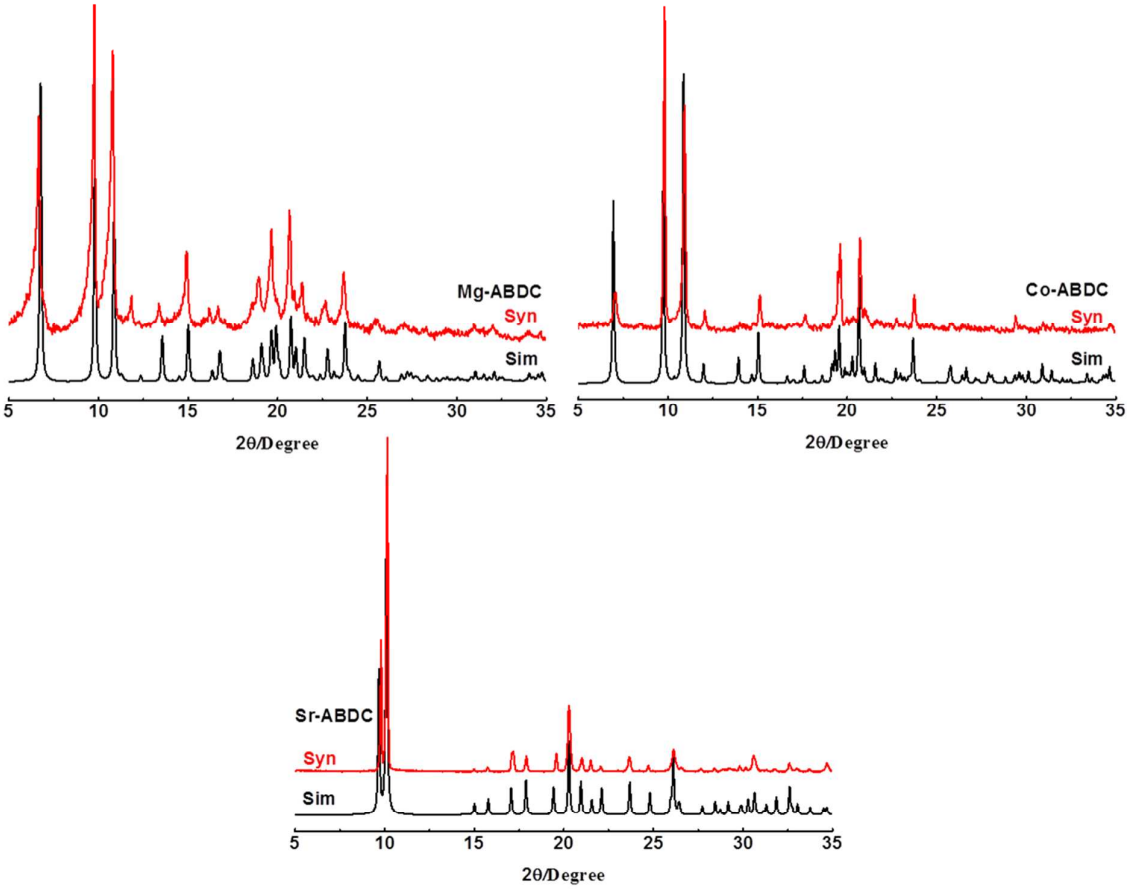

Fig. 3 Comparison of XRD patterns from synthesis (red) and simulation (black).

Fig. 3 shows XRD patterns of the M-ABDC samples prepared in the experiments and XRD patterns of model M-ABDC structures predicted from the SXRD calculations. The similarities in the two sets of patterns indicate that the Mg-ABDC, Co-ABDC and Sr-ABDC prepared in this study have a high degree of purity. The powder XRD patterns of Mg-ABDC and Co-ABDC both have similar features that confirm these materials have isoreticular frameworks, and that the Mg- and Co-frameworks have similar pore shapes and sizes. The XRD pattern of Sr-ABDC is similar to the pattern reported by Liang et al. for a calcium-based MOF [Ca(ABDC)(DMF)].[45]

3.4. Thermal stability of M-ABDC (M = Mg, Co, Sr)

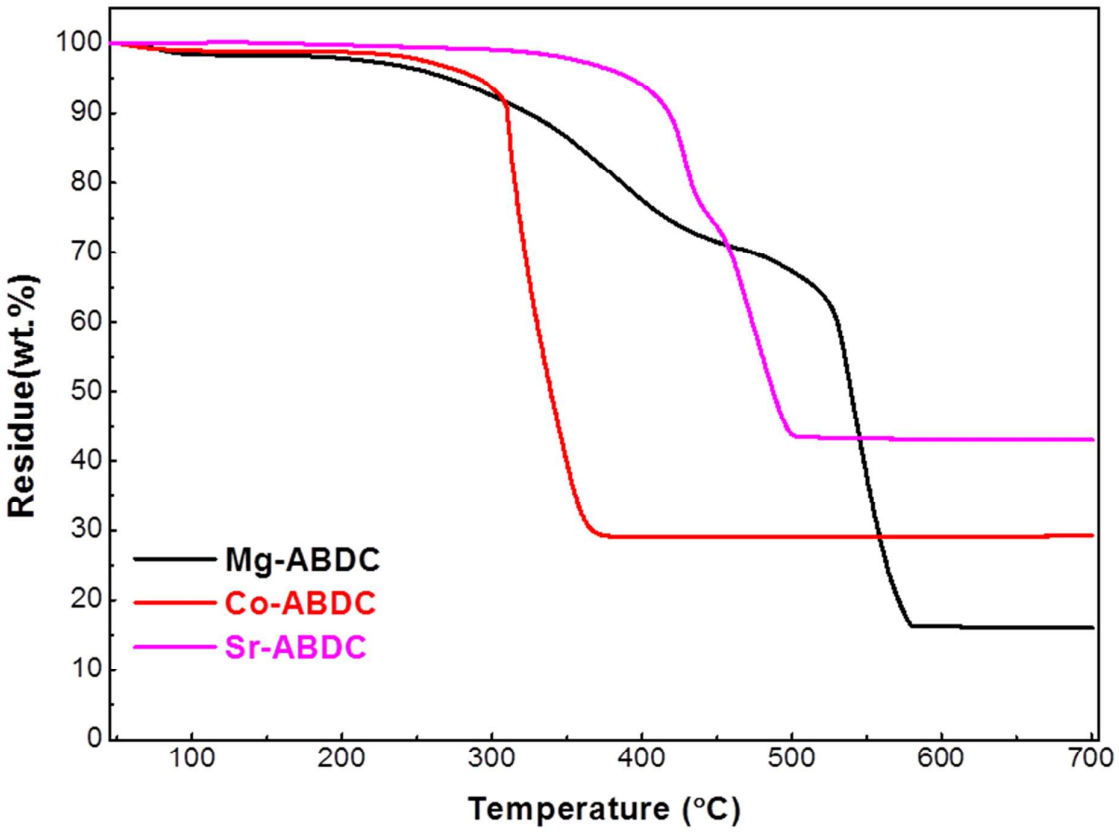

Fig. 4 Weight loss (TGA) curves of Mg-ABDC, Co-ABDC and Sr-ABDC measured in air at a heating rate of 5 °C/min

All three M-ABDC samples were thermally stable up to temperatures of 300 °C (Fig. 4), with the Sr-ABDC still being stable at 400 °C. Notably, the decomposition of Sr-ABDC was at a higher temperature than that observed for ZIF-8, another widely studied MOFs material with the decomposition temperature at approximately 380 °C.[47-49] The weight losses observed in Mg-ABDC and Co-ABDC at temperatures below 100 °C are due to the evaporation of surface-adsorbed DMF, methanol and moisture. The decompositions of these frameworks were completed at temperatures of 370 °C, 500 °C and 575 °C for Co-ABDC, Sr-ABDC, Mg-ABDC, respectively. Though Mg-ABDC and Co-ABDC have different decomposition terminal temperatures, however the initial decomposition temperatures are similar (above

300°C). Co-ABDC exhibits a rapid weight loss above 300 °C, indicating the fast decomposition of MOF structure. As to Mg-ABDC, gradual weight loss (>20%) happened from 300 °C to 540 °C following by a sharp weight drop above 540 °C, suggesting a two-step decomposition.

3.5. Surface area and porosity of M-ABDC (M = Mg, Co, Sr)

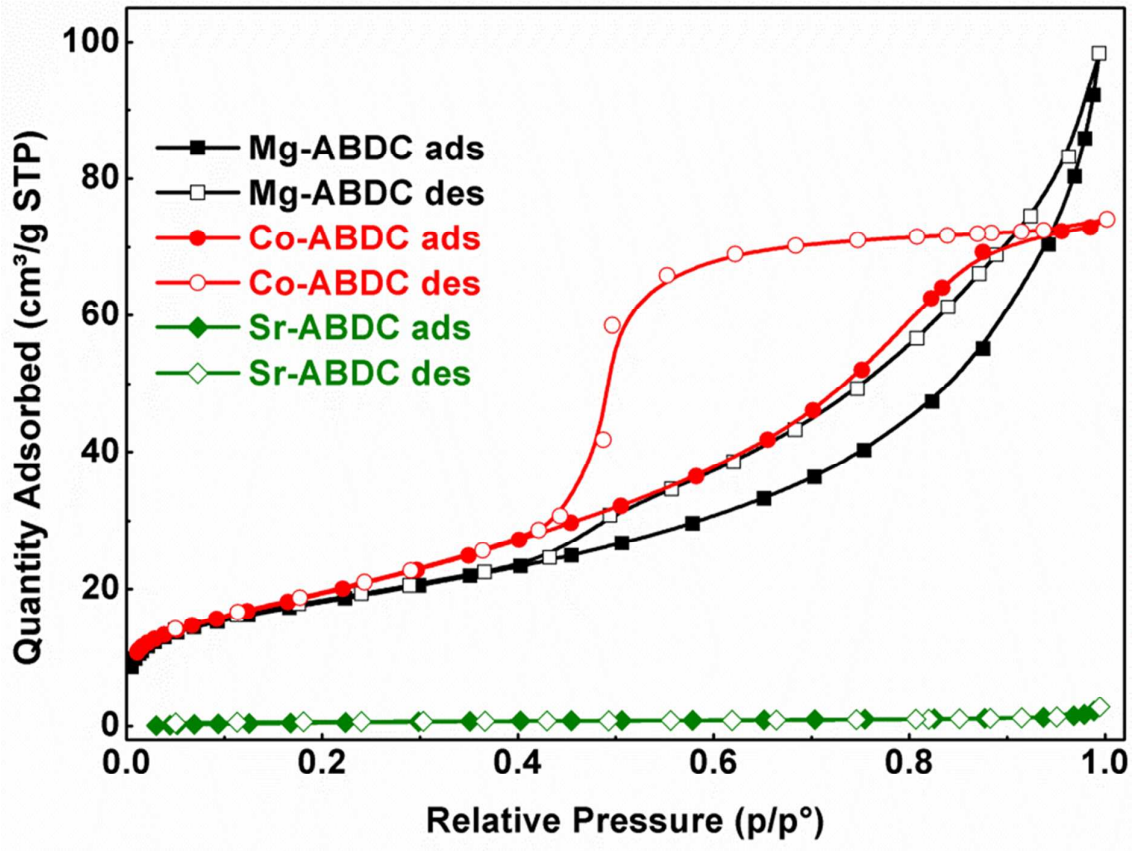

Fig. 5 N_2 ads-desorption isotherms measured at -196 °C.

Fig. 5 presents N_2 sorption isotherms for Mg-ABDC, Co-ABDC and Sr-ABDC measured at -196 °C. Specific surface areas and pore volumes are listed in Table 3. The low surface area and small pore volume of Sr-ABDC obtained from N_2 sorption analyses may be not an accurate measure of the pore structure, because the transport of the N_2 probe molecule (kinetic diameter 3.64 Å) is kinetically restricted in the narrow rhomboidal channels

(4.6×3.6 $Å^2$) of Sr-ABDC. The Mg-ABDC and Co-ABDC exhibit moderate uptakes of N_2 at relative pressures less than $P/P_0 = 0.2$ with hysteresis loops at $P/P_0 \approx 0.45$-0.90. The hysteresis loop is probably due to strong fluid-solid attractive interaction in adsorption process[50] or the formation of some mesopores in activation process. These isotherms are described as Type IV according to the IUPAC classifications.[51] Table 3 shows that the pore volumes measured by N_2 sorption are significantly smaller than theoretical values calculated from the SXRD data (for example Mg-ABDC 0.152 cm^3/g by N_2 sorption; 0.402 cm^3/g from the SXRD model), and these differences may be explained by existence of residual guest molecules that reduce the MOFs capacity for N_2 sorption. These results are consistent with other reports that concluded the adsorption properties (adsorption capacity, surface area and pore volume) of MOFs containing bound guest molecules are highly dependent upon the desolvation conditions.[5, 33, 34]

Table 3 BET surface area and pore volume (Experiment) determined from N_2 sorption isotherms. Pore volume calculated SXRD structural model.

Sample	S_{BET} (m^2/g)	*Pore volume*(cm^3/g) (Experiment)	*Pore volume*(cm^3/g) (Calculated)
Mg-ABDC	63	0.152	0.402
Co-ABDC	71	0.114	0.318
Sr-ABDC	2.5	0.004	0.206

3.6. CO_2 and N_2 equilibrium adsorption capacities of M-ABDC (M = Mg, Co, Sr)

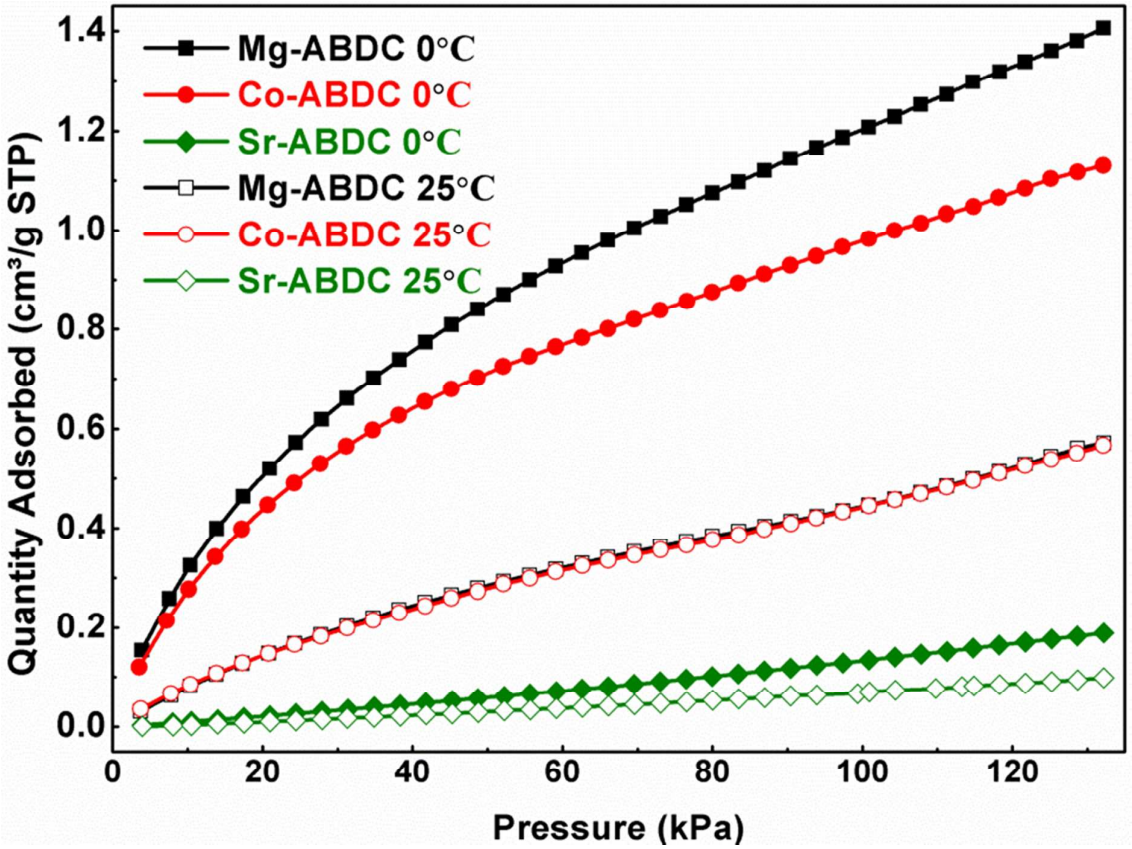

Fig. 6 CO_2 adsorption at 0 °C and 25 °C on M-ABDC (M = Mg, Co, Sr).

Fig. 6 shows CO_2 equilibrium adsorption capacities measured at 0 °C and 25 °C and pressures from 3.5 to 132 kPa. N_2 adsorption isotherms at 0 °C are included in the Supporting Information (Fig. S1). The Langmuir isotherm model was fitted to the CO_2 and N_2 data with best fit parameters listed in Table S1. The CO_2 capacities temperature 0 °C and pressure 132 kPa were 1.406, 1.131 and 0.189 mmol/g for Mg-ABDC, Co-ABDC, Sr-ABDC, respectively. This trend is consistent with the order of surface area and pore volume. But the ionic character of Mg-O bond is also favorable for CO_2 uptake.[35] The low CO_2 uptake on Sr-ABDC is due to small pore volume, narrow pore throats, and weak ionic character of the Sr-O bonds. The N_2 adsorption capacities of Mg-ABDC, Co-ABDC and Sr-ABDC at 0 °C and 132 kPa are 0.106, 0.110 and 0.099 mmol/g, respectively. Ideal equilibrium selectivity for

CO_2 over N_2, calculated using Langmuir isotherms parameters[52, 53], were 396 for Mg-ABDC, 326 for Co-ABDC and 18 for Sr-ABDC.

To evaluate the interactions between CO_2 molecules and the frameworks structure, the isosteric heat of CO_2 adsorption (Q_{st}) was calculated by the Clausius-Clapeyron equation from adsorption isotherms at 0 and 25 °C. The Q_{st} values of Mg-ABDC and Co-ABDC (Fig. S3) were much higher than those of Sr-ABDC due to the difference in the ionic character of the metal-oxide bonds.[35, 42] The Mg-O bonds in Mg-ABDC and the Co-O bonds in Co-ABDC have higher ionic character than the Sr-O bonds in Sr-ABDC, leading to a higher positive charge density on Mg^{2+} and Co^{2+} metal centers. In contrast to Mg-ABDC, higher isosteric heats of CO_2 adsorption at low surface coverage on Co-ABDC is attributed to the higher ionic character of Co-O bonds in Co-ABDC. It is worth noting that the Q_{st} values of Sr-ABDC decreased significantly as adsorption uptakes increased, which is attributed to small pore channels, low void space as well as weak ionic character.

To further evaluate the selectivity of CO_2 over N_2 for Mg-ABDC and Co-ABDC for a gas mixture, ideal adsorbed solution theory (IAST) was applied to predict the binary-component adsorption performance and selectivities for CO_2+N_2 mixtures. The detailed procedures and fitting parameters are presented in the Supporting Information. Fig. S4 exhibits the predicted adsorption selectivities of Mg-ABDC and Co-ABDC for equimolar CO_2+N_2 mixture as a function of total bulk pressure. Both frameworks exhibit very high initial selectivity of CO_2/N_2 (>375) in an equimolar mixture, and then the selectivity decreased significantly with the increase of pressure. The adsorption performances of these new MOFs in this study are compared with some reported MOFs containing LBSs or/and OMSs in terms of surface area, adsorption capacity and selectivity of CO_2/N_2 (Table S3). Though the surface area and adsorption capacity of Mg-ABDC and Co-ABDC are limited by the residual solvent, the polar pore structures of the frameworks in which the -NH_2 groups of H_2ABDC together with

the coordinated unsaturated Mg(II) and Co(II) centers provide stronger affinity for CO_2 molecules than N_2 molecules, resulting to the remarkably high CO_2/N_2 selectivity. The high selectivity of CO_2 over N_2 may promote Mg-ABDC and Co-ABDC as desirable adsorbent materials for separation of CO_2 and N_2 in flue gas.

4. Conclusions

Three new amino-functionalized MOFs with OMSs have been prepared from the solvothermal reactions of 2-aminoterephthalic acid with Mg(II), Co(II) and Sr(II) ions. The trimetallic SBUs in both Mg-ABDC and Co-ABDC are connected through dicarboxylate ligands to form 2D layer structure, while the chain-like SBUs in Sr-ABDC are connected by eight-coordinated Sr(II) ions to provide 3D channel structure. In all three frameworks, the pore surface is decorated by the $-NH_2$ groups (LBSs) and the OMSs are created upon the removal of coordinated DMF molecules. Sr-ABDC was the most thermal stable framework. Mg-ABDC and Co-ABDC exhibited higher BET surface area, pore volume and gas uptakes than Sr-ABDC. Moreover, Mg-ABDC and Co-ABDC display high heat of adsorption for CO_2 and high CO_2/N_2 selectivity. IAST also predicts high selectivities for CO_2+N_2 mixtures. The observed strong binding affinity for CO_2 can be attributed to the OMSs and $-NH_2$ groups in Mg-ABDC and Co-ABDC. Other efficient activation processes are desired to improve the surface area and adsorption capacity without destroying framework structure.

Supporting Information Available

Crystallographic information files (CIF); N_2 adsorption isotherms at 25 °C; Langmuir constants of CO_2 and N_2 adsorption at 0 °C and selectivity of CO_2/N_2; CO_2/N_2 selectivity prediction via IAST; Isosteric heats of CO_2 adsorption calculated by Clausius-Clapeyron equation based on adsorption isotherms at 0 °C and 25 °C; IAST adsorption isotherms of CO_2+N_2 mixture at 50/50 and selectivities of Mg-ABDC and Co-ABDC; BET surface area,

CO_2 adsorption capacity and selectivity of some reported MOFs containing LBSs or/and OMSs.

AUTHOR INFORMATION

Corresponding Author

*Email: z.zhu@uq.edu.au (Z Zhu) and l.ge@uq.edu.au (L Ge)

Notes

The authors declare no competing financial interest.

ACKNOWLEDGMENTS

Zhonghua Zhu acknowledges the finance support by the Australian Research Council Future Fellowship Project FT120100720. Ying Yang also likes to thank the financial support from the China Scholarship Council (CSC).

References

1 C. D. Keeling, T. P. Whorf, M. Wahlen and J. van der Plichtt, *Nature*, 1995, **375**, 666-670.
2 T. R. Karl and K. E. Trenberth, *Science*, 2003, **302**, 1719-1723.
3 J.-R. Li, J. Sculley and H.-C. Zhou, *Chem. Rev.*, 2012, **112**, 869-932.
4 H. L. Jiang and Q. Xu, *Chem. Commun.*, 2011, **47**, 3351-3370.
5 K. Sumida, D. L. Rogow, J. A. Mason, T. M. McDonald, E. D. Bloch, Z. R. Herm, T.-H. Bae and J. R. Long, *Chem. Rev.*, 2011, **112**, 724-781.
6 S. Couck, J. F. M. Denayer, G. V. Baron, T. Rémy, J. Gascon and F. Kapteijn, *J. Am. Chem. Soc.*, 2009, **131**, 6326-6327.
7 S. S.-Y. Chui, S. M.-F. Lo, J. P. H. Charmant, A. G. Orpen and I. D. Williams, *Science*, 1999, **283**, 1148-1150.
8 M. Eddaoudi, J. Kim, N. Rosi, D. Vodak, J. Wachter, M. O'Keeffe and O. M. Yaghi, *Science*, 2002, **295**, 469-472.
9 S. Bauer, C. Serre, T. Devic, P. Horcajada, J. Marrot, G. Férey and N. Stock, *Inorg. Chem.*, 2008, **47**, 7568-7576.
10 T. Ahnfeldt, D. Gunzelmann, T. Loiseau, D. Hirsemann, J. r. Senker, G. Férey and N. Stock, *Inorg. Chem.*, 2009, **48**, 3057-3064.
11 S. J. Garibay and S. M. Cohen, *Chem. Commun.*, 2010, **46**, 7700-7702.
12 A. Torrisi, C. Mellot-Draznieks and R. G. Bell, *Cryst. Growth Des.*, 2010, **10**, 2839-2841.
13 P. Serra-Crespo, E. V. Ramos-Fernandez, J. Gascon and F. Kapteijn, *Chem. Mater.*, 2011, **23**, 2565-2572.
14 X. Y. Chen, H. Vinh-Thang, D. Rodrigue and S. Kaliaguine, *Ind. Eng. Chem. Res.*, 2012, **51**, 6895-6906.
15 B. Yuan, D. Ma, X. Wang, Z. Li, Y. Li, H. Liu and D. He, *Chem. Commun.*, 2012, **48**, 1135-1137.

16 J.-R. Li, Y. Ma, M. C. McCarthy, J. Sculley, J. Yu, H.-K. Jeong, P. B. Balbuena and H.-C. Zhou, *Coord. Chem. Rev.*, 2011, **255**, 1791-1823.

17 Z. Zhang, Y. Zhao, Q. Gong, Z. Li and J. Li, *Chem. Commun.*, 2013, **49**, 653-661.

18 S. Chaemchuen, N. A. Kabir, K. Zhou and F. Verpoort, *Chem. Soc. Rev.*, 2013, **42**, 9304-9332.

19 C.-B. Liu, X.-J. Zheng and L.-P. Jin, *J. Chem. Crystallogr.*, 2006, **36**, 199-204.

20 J. L. C. Rowsell and O. M. Yaghi, *J. Am. Chem. Soc.*, 2006, **128**, 1304-1315.

21 M. Anbia and V. Hoseini, *J. Nat. Gas Chem.*, 2012, **21**, 339-343.

22 J. Sienkiewicz-Gromiuk, L. Mazur, A. Bartyzel and Z. Rzączyńska, *J. Inorg. Organomet. Polymer Mater.*, 2012, **22**, 1325-1331.

23 A. R. Millward and O. M. Yaghi, *J. Am. Chem. Soc.*, 2005, **127**, 17998-17999.

24 S. Couck, J. F. M. Denayer, G. V. Baron, T. Rémy, J. Gascon and F. Kapteijn, *J. Am. Chem. Soc.*, 2009, **131**, 6326-6327.

25 Q. Yang, A. D. Wiersum, P. L. Llewellyn, V. Guillerm, C. Serre and G. Maurin, *Chem. Commun.*, 2011, **47**, 9603-9605.

26 Y. Zhao, H. Zeng, J. Li, H. Wu, T. J. Emge, Q. Gong, N. Nijem, Y. J. Chabal, L. Kong, D. C. Langreth and H. Liu, *Chemistry (Weinheim an der Bergstrasse, Germany)*, 2011, **17**, 5101-5109.

27 D. Farrusseng, C. c. Daniel, C. Gaudillère, U. Ravon, Y. Schuurman, C. Mirodatos, D. Dubbeldam, H. Frost and R. Q. Snurr, *Langmuir*, 2009, **25**, 7383-7388.

28 A. Vimont, J.-M. Goupil, J.-C. Lavalley, M. Daturi, S. Surblé, C. Serre, F. Millange, G. Férey and N. Audebrand, *J. Am. Chem. Soc.* , 2006, **128**, 3218-3227.

29 M. Dincă and J. R. Long, *Angew. Chem. Int. Ed.*, 2008, **47**, 6766-6779.

30 W. Zhou, H. Wu and T. Yildirim, *J. Am. Chem. Soc.*, 2008, **130**, 15268-15269.

31 P. D. C. Dietzel, V. Besikiotis and R. Blom, *J. Mater. Chem.*, 2009, **19**, 7362-7370.

32 B. Chen, S. Xiang and G. Qian, *Acc. Chem. Res.*, 2010, **43**, 1115-1124.

33 J. Liu, J. T. Culp, S. Natesakhawat, B. C. Bockrath, B. Zande, S. G. Sankar, G. Garberoglio and J. K. Johnson, *J. Phys. Chem. C*, 2007, **111**, 9305-9313.

34 Y. Yang, P. Shukla, S. Wang, V. Rudolph, X.-M. Chen and Z. Zhu, *RSC Adv.*, 2013, 3, 17065-17072.

35 S. R. Caskey, A. G. Wong-Foy and A. J. Matzger, *J. Am. Chem. Soc.*, 2008, **130**, 10870-10871.

36 P. D. C. Dietzel, Y. Morita, R. Blom and H. Fjellvåg, *Angew. Chem. Int. Ed.* , 2005, **44**, 6354-6358.

37 P. D. C. Dietzel, B. Panella, M. Hirscher, R. Blom and H. Fjellvag, *Chem. Commun.*, 2006, **9**, 959-961.

38 N. L. Rosi, J. Kim, M. Eddaoudi, B. Chen, M. O'Keeffe and O. M. Yaghi, *J. Am. Chem. Soc.*, 2005, **127**, 1504-1518.

39 P. D. C. Dietzel, R. Blom and H. Fjellvåg, *Eur. J. Inorg. Chem.*, 2008, **23**, 3624-3632.

40 K. Sumida, C. M. Brown, Z. R. Herm, S. Chavan, S. Bordiga and J. R. Long, *Chem. Commun.*, 2011, **47**, 1157-1159.

41 J. Liu, A. I. Benin, A. M. Furtado, P. Jakubczak, R. R. Willis and M. D. LeVan, *Langmuir*, 2011, **27**, 11451-11456.

42 A. O. z. r. Yazaydın, R. Q. Snurr, T.-H. Park, K. Koh, J. Liu, M. D. LeVan, A. I. Benin, P. Jakubczak, M. Lanuza, D. B. Galloway, J. J. Low and R. R. Willis, *J. Am. Chem. Soc.*, 2009, **131**, 18198-18199.

43 G. M. Sheldrick, *Acta Crystallogr. Sec. A*, 2008, **64**, 112-122.

44 C. F. Macrae, P. R. Edgington, P. McCabe, E. Pidcock, G. P. Shields, R. Taylor, M. Towler and J. van de Streek, *J. Appl. Crystallogr.*, 2006, **39**, 453-457.

45 P.-C. Liang, H.-K. Liu, C.-T. Yeh, C.-H. Lin and V. t. z. Zima, *Cryst. Growth Des.*, 2011, 11, 699-708.

46 A. L. Spek, *J. Appl. Crystallogr.*, 2003, **36**, 7-13.

47 X.-C. Huang, Y.-Y. Lin, J.-P. Zhang and X.-M. Chen, *Angew. Chem. Int. Ed.*, 2006, **45**, 1557-1559.

48 J. Cravillon, S. Münzer, S.-J. Lohmeier, A. Feldhoff, K. Huber and M. Wiebcke, *Chem. Mater.*, 2009, **21**, 1410-1412.

49 Y. Yang, L. Ge, V. Rudolph and Z. Zhu, *Dalton Trans.*, 2014, **43**, 7028-7036.

50 K. S. W. Sing, D. H. Everett, R. A. W. Haul, L. Moscou, R. A. Pierotti, J. Rouquerol and T. Siemieiewska, *Pure Appl. Chem.*, 1985, **57**, 603-619.

51 D. H. Everett, *Pure Appl. Chem.*, 1972, **31**, 578-638.

Table of contents

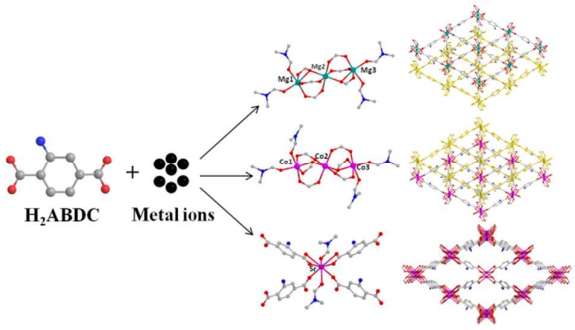

Three new amino-functionalized MOFs based on 2-aminoterephthalic acid with Mg(II), Co(II) and Sr(II) ions.